AI-GAN: SIGNAL DE-INTERFERENCE VIA ASYNCHRONOUS INTERACTIVE GENERATIVE ADVERSARIAL NETWORK

Xin Jin *Zhibo Chen** *Jianxin Lin* *Wei Zhou* *Jiale Chen* *Chaowei Shan*

CAS Key Laboratory of Technology in Geo-spatial Information Processing and Application System, University of Science and Technology of China, Hefei, China

ABSTRACT

Interfering signals, such as rain streak, haze, noise, etc, introduce various types of visibility degradation on original clean signals. Traditional algorithms tackle the signal de-interference problem by the way of signal removal, which usually causes over-smoothness and unexpected artifacts. Hereby, this paper attempts to solve this problem from a totally different perspective of signal decomposition, and introduces the interaction and constraints between the two decomposed signals during the restoration procedure. Specifically, we propose an Asynchronous Interactive Generative Adversarial Network (AI-GAN), which decomposes the degraded signal into original and interfering parts progressively through a double branch structure. Each branch employs an asynchronous synthesis strategy for the corresponding generator and interacts with each other by exchanging the feedforward signal values and sharing the corresponding feedback gradients, achieving an effect of mutual adversarial optimization. The proposed AI-GAN shows significant qualitative and quantitative improvement on general signal de-interference tasks such as deraining, dehazing, and denoising.

***Index Terms*—** Signal de-interference, signal decomposition, asynchronous and interactive, double branch, GANs

1. INTRODUCTION

Unpredictable interfering signals, such as rain streak, haze, and Gaussian noise, adversely affect the performance of many intelligent signal processing systems, such as surveillance system, autonomous car, unmanned aerial vehicle (UAV), etc. Hence, a general and effective signal de-interference algorithm is urgently needed.

In this paper, we focus on the image signal de-interference field, which is more challenging due to the diversity of interfering signals and the complex entanglement between interfering and original image signals. Traditional de-interference methods usually suffer from the over-smoothness and unexpected artifacts, because they tend to regard the signal de-interference task as a simple signal removal problem [1, 2, 3]. Meanwhile, convolutional neural networks (CNNs) have shown their superior performance in many image de-interference fields, such as deraining [4, 5, 6], dehazing [7, 8, 9], and denoising [10, 11, 12]. However, existing CNN-based methods typically follow the same basic idea of signal removal and only focus on a specific type of interfering signal, they almost lack the consideration for the common nature behind different interference. In this paper, we try to understand the image de-interference problem from a new perspective of signal decomposition, and explore the interdependency between two decomposed signals in an interactive manner, as shown in Figure 1. Specifically, we propose an end-to-end learning-based model named Asynchronous Interactive Generative Adversarial Network (AI-GAN), which decomposes the degraded signal into original and interfering parts progressively through a double branch structure. Each branch employs an asynchronous synthesis strategy and interacts with each other, achieving an effect of mutual adversarial optimization and achieving the purpose of de-interference. The contributions of this paper are summarized as follows:

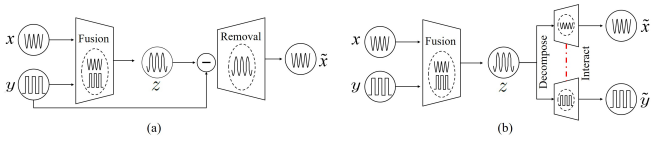

Fig. 1. Comparison between the common model and our model. x, y, z denote original, interfering, and degraded signal, respectively. (a) Regard signal de-interference as simple signal removal. (b) We model signal de-interference problem from the respective of signal interactive decomposition.

- We redefine the problem of image signal de-interference from a totally different perspective of signal decomposition, and handle different types of interfering signals in an interactive manner.
- We propose an end-to-end learning network AI-GAN, which decomposes the degraded signal into original and interfering parts progressively through a double branch structure. Each branch employs an asynchronous synthesis strategy and interacts with each

*Corresponding author. (E-mail: chenzhibo@ustc.edu.cn)

other in an adversarial manner, which achieves a mutual promotion effect and outputs realistic restored original signals and interfering signals simultaneously.

- Extensive experiments have demonstrated that AI-GAN has a strong generalization ability to deal with different types of interfering signals on the image, such as deraining, dehazing, and denoising.

2. RELATED WORK

Traditional Methods: For deraining, traditional methods generally employ different mathematical models to handle the degraded rainy images [2, 3]. Recently, some algorithms have described the image deraining as a layer separation task. Luo et al. [3] use a discriminative sparse coding method to recover the original clean images. Li et al. [13] exploit the Gaussian mixture model to remove the rain streaks, and patch-based priors are used for both a clean layer and a rain layer. For dehazing, He et al. [14] discover Dark Channel Prior (DCP) based on empirical statistics of experiments on haze-free images. With dark channel prior, the thickness of haze is estimated and removed by the atmospheric scattering model. However, DCP loses dehazing quality in the sky images and is computationally intensive. Meng et al. [15] propose an effective regularization dehazing method to restore the haze-free image by exploring the inherent boundary constraint. For denoising, traditional methods, such as classic BM3D algorithm [16] and dictionary learning based methods [17] show good performance on image denoising. Since it is an ill-posed problem, the use of regularization EPLL [18] and WNNM [19] are proved to be essential.

Deep Neural Network: The renaissance of DNN remarkably accelerates the progress of many computer vision tasks, ranging from high-level recognition/translation [20] to low-level denoising/restoration [21, 8, 22]. For deraining, Eigen et al. [23] try to propose a CNN-based rain removal solution but have got unsatisfactory results. Recently, inspired by the deep residual learning, Fu et.al. [5] simplify the learning process by changing the mapping form and focusing on the high-frequency details (Detail-Net) during training. Yang et al. [6] propose a deep recurrent rain removal network (JORDER) to remove rain streaks iteratively. Zhang et.al. [24] present a density-aware multi-stream connected network called DID-MDN for joint rain density estimation and deraining. For dehazing, Cai et al. [7] propose a CNN-based image dehazing method, named DehazeNet, where a regressor is trained to predict the medium transmission. Similar with DehazeNet [7], Ren et al. [8] design a multi-scale CNN (MSCNN) for single image dehazing. Recently, Li et al. [9] propose an all-in-one deep model (AOD-Net) for single image dehazing, which directly generates the clean image using CNN. For denoising, Xie et al. [10] combine sparse coding and pre-trained DNN with denoising auto-encoder for this low-level vision task. Other DNN-based methods such as [11] and DnCNN [12] for image denoising have been actively studied recently.

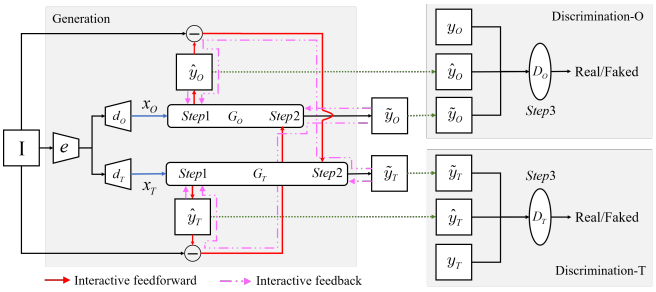

Fig. 2. Structure of the proposed Asynchronous Interactive Generative Adversarial Network (AI-GAN) for signal de-interference. The final output includes two components: the asynchronous fusion of $\hat{y}_O$ and $\tilde{y}_O$ for original signal; the asynchronous fusion of $\hat{y}_T$ and $\tilde{y}_T$ for interfering signal.

3. ASYNCHRONOUS INTERACTIVE GAN (AI-GAN)

3.1. Asynchronous and Interactive Architecture

AI-GAN is based on an asynchronous and interactive double branch architecture. One branch generates original image signal, and the other generates interfering signal. As shown in Figure 2, AI-GAN consists of one common encoder e, two decoders (i.e. d_O, d_T), two pairs of GANs (i.e. generators G_O, G_T and discriminators D_O, D_T).

Feature Extraction: The common encoder e first extracts the common features from degraded input I, and then two independent decoders d_O, d_T respectively disentangle common features to generate two kinds of features: original features x_O and interfering features x_T. In particular, given a degraded image I as input, we have:

$$x_O = d_O(e(\mathrm{I})); \qquad x_T = d_T(e(\mathrm{I})) \tag{1}$$

Asynchronous synthesis and Interaction: Then generators G_O and G_T take the original features x_O and the interfering features x_T as inputs respectively, as the blue arrows denoted in Figure 2, and output the first-step image generation (i.e. $Step1$ in Figure 2) separately:

$$\hat{y}_O = G_O(x_O); \qquad \hat{y}_T = G_T(x_T). \tag{2}$$

Subsequently, in asynchronous moments of time, G_O and G_T interact with each other based on the first-step generation results $\hat{y}_O$ and $\hat{y}_T$, which is denoted by red arrows in Figure 2. Specifically, G_O and G_T receive again the residuals of I - $\hat{y}_T$ and I - $\hat{y}_O$ as inputs respectively, and output the second-step generation results $\tilde{y}_O$ and $\tilde{y}_T$ (i.e. $Step2$ in Figure 2):

$$\tilde{y}_O = G_O(\mathrm{I} - \hat{y}_T); \qquad \tilde{y}_T = G_T(\mathrm{I} - \hat{y}_O). \tag{3}$$

We argue that the interaction can assist G_O and G_T to additionally learn two mappings: from I - $\hat{y}_T$ to $\tilde{y}_O$, and from I - $\hat{y}_O$ to $\tilde{y}_T$. This interdependency relationship allows G_O and G_T mutually benefit and constraint with each other by exchanging the feed-forward values and sharing the corresponding feedback gradients during the optimization process, reaching a win-win effect ultimately.

3.2. Mutual Adversarial Optimization Mechanism

Inspired by [25], we propose a more generalized mutual adversarial optimization mechanism to jointly optimize two generators of AI-GAN, which is achieved by a hybrid loss function and two independent discriminators D_O, D_T. We validate the effectiveness of the mutual adversarial optimization mechanism in the following ablation study section.

The proposed hybrid loss function consists of the Interact Loss and the GAN Loss. The key idea of Interact Loss is to improve the performance of two generators by minimizing the square errors between synthesized results and targets (i.e. y_O, y_T), which includes two asynchronous components, namely the first-step reconstruction error $\mathcal{L}_{\text{MSE-Step1}}$ and the second-step reconstruction error $\mathcal{L}_{\text{MSE-Step2}}$:

$$\mathcal{L}_{\text{MSE-Step1}} = \|G_O(x_O) - y_O\|^2 + \|G_T(x_T) - y_T\|^2, \quad (4)$$

$$\mathcal{L}_{\text{MSE-Step2}} = \|G_O(\text{I}-\hat{y}_T)-y_O\|^2+\|G_T(\text{I}-\hat{y}_O)-y_T\|^2, \quad (5)$$

$$\mathcal{L}_{\text{Interact}} = \mathcal{L}_{\text{MSE-Step1}} + \mathcal{L}_{\text{MSE-Step2}}. \quad (6)$$

$\mathcal{L}_{Interact}$ allows the generators G_O and G_T to interact with each other through asynchronous and symmetric feedback gradients during the back-propagation, which is denoted by purple dotted arrows in Figure 2. The synthesized original signal assists to infer interfering signal, while the synthesized interfering signal in turn leads to the realistic original signal, which makes each generator to learn the corresponding mapping well and to reach a generalized adversarial effect. In addition, the generators G_O, G_T try to minimize the whole objective function against the discriminators D_O, D_T that try to maximize it. D_O and D_T learn to distinguish real signals from the generated ones which are obtained at asynchronous time points (i.e. $Step3$ in Figure 2). Then we further update the parameters of two branches asynchronously through the following GAN Loss, namely $\mathcal{L}_{\text{GAN-O}}$ and $\mathcal{L}_{\text{GAN-T}}$:

$$\begin{aligned}\mathcal{L}_{\text{GAN-O}} = &\log(D_O(y_O)) + \log(1 - D_O(G_O(x_O))) \\ &+ \log(1 - D_O(G_O(\text{I} - \hat{y}_T))),\end{aligned} \quad (7)$$

$$\begin{aligned}\mathcal{L}_{\text{GAN-T}} = &\log(D_T(y_T)) + \log(1 - D_T(G_T(x_T))) \\ &+ \log(1 - D_T(G_T(\text{I} - \hat{y}_O))).\end{aligned} \quad (8)$$

In summary, the generators G_O, G_T and the discriminators D_O, D_T form a closed-loop structure together, which enables each branch of AI-GAN to share effective information during optimization procedure, reaching a win-win result ultimately. $\lambda = 0.8$ balances the Interact Loss and GAN Loss.

$$\begin{aligned}\min_{G_O,G_T}\max_{D_O,D_T} \mathcal{L}_{\text{Interact}}(G_O, G_T) + \lambda(\mathcal{L}_{\text{GAN-O}}(G_O, D_O) \\ +\mathcal{L}_{\text{GAN-T}}(G_T, D_T)).\end{aligned} \quad (9)$$

3.3. Discussions

To demonstrate the effectiveness of the asynchronous and interactive double branch structure and visually highlight the differences between a standard single-branched GAN and the proposed AI-GAN, we design an illustrative toy experiment based on 1-dimensional synthetic sampling data. Two 1-dimensional independent Gaussian signals A & B has been introduced, and we take their fusion signal that belongs to a Gaussian mixture model as input signal C.

The left-most picture in Figure 3 shows the initial state of toy experiment where three color curves represent the histograms of different signals. Gaussian signal B (orange curve) is target data sample, our goal is to restore B from mixture data samples C (green curve) where signal A (blue curve) is viewed as interfering data sample.

As shown in Figure 3 (b), in the baseline (standard single-branched GAN) case, there is a large gap between the histogram of the synthesized result (red curve) and the target histogram (orange curve). This indicates that the result fails to cover all distributions in target signal B. On the contrary, refer to Figure 3 (c), our model is able to not only fit signal A (purple curve) and signal B (red curve) efficiently at the same time, but also can fit the target signal B more accurately than single-branch methods. Furthermore, the loss function curve in Figure 3 (d) also illustrates that our generator for target data reach the global optimum more quickly than that in single-branched GAN, which clearly support the superiority of our proposed asynchronous and interactive double branch structure over standard single-branched GAN.

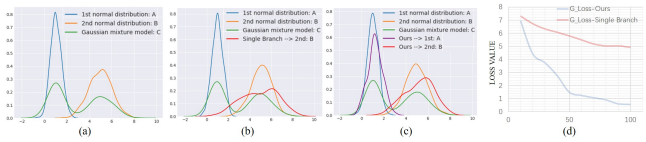

Fig. 3. Toy domain experiment results. The different color histogram curves show the situation of different signals. (a) the initial state of toy experiment, (b) the standard single-branched GAN model, (c) our proposed model, (d) the loss curves of two models' generators.

Table 1. Average PSNR and SSIM results on Rain100L and Rain100H. *Italics* represent three ablated baselines.

	PSNR									
	ID	DSC	LP	Detail-Net	JORDER	DID-MDN	*S-GAN*	*D-GAN*	*AI-CNN*	**AI-GAN**
Rain100L	27.21	30.02	32.02	33.75	36.02	36.14	35.07	34.95	36.09	**37.56**
Rain100H	14.02	15.66	14.26	21.82	23.45	26.69	25.45	25.11	26.23	**27.72**
	SSIM									
Rain100L	0.756	0.877	0.961	0.931	0.961	0.972	0.943	0.941	0.968	**0.987**
Rain100H	0.523	0.541	0.427	0.744	0.753	0892	0.875	0.851	0.886	**0.931**

Fig. 4. Results of different methods on rainy images. From left to right: rainy image, Detail-Net [5], JORDER [6] DID-MDN [24] and our AI-GAN. Note that the image contents in the red boxes are enlarged and shown below the corresponding images.

4. EXPERIMENTS

In this section, we provide the evaluation of deraining, dehazing, and denoising performance of the AI-GAN against a few existing state-of-the-art methods. Deraining experiments are performed on two synthetic datasets as well as a real-world dataset: Rain100L and Rain100H [5, 6]; Real-world dataset includes 20 real rain images with various types of rain streaks. We compare our method with state-of-the-art deraining methods: image decomposition (ID) [2], layer priors (LP) [13], discriminative sparse coding (DSC) [3], deep detail network (Detail-Net) [5], JORDER [6] and DID-MDN [24].

For dehazing, we also test synthetic [1] and natural hazy images with DCP [14], DehazeNet [7], MSCNN [8], AOD-Net [9] and our model under the same environment.

For denoising, we test additive Gaussian noises with zero mean and standard deviation σ = 15, 25 and 50 respectively on the Berkeley segmentation dataset (BSD68). BM3D [16], EPLL [18], WNNM [19] and DnCNN [12] are compared with our method under the same environment.

Peak Signal-to-Noise Ratio (PSNR) and Structural SIMilarity (SSIM) index are calculated for quantitative evaluation.

4.1. Image Deraining

Evaluation on Rain100L and Rain100H: Table 1 shows the results of different methods on Rain100L (L: light rainy) and Rain100H (H: heavy rainy). We can observe that the proposed AI-GAN significantly outperforms other models in terms of both PSNR and SSIM, especially in heavy rainy cases. AI-GAN gains over 1.0 dB in PSNR than other state-of-the-art methods on Rain100H, such a large gain strongly demonstrates that the asynchronous and interactive double branch structure with a mutual adversarial optimization mechanism significantly boosts the performance.

Evaluation on Real-world Test Data: The qualitative comparison picture in Figure 4 shows the visual restored results. Detail-Net [5] leaves residual rain streaks in the background because they only adopt signal-removal measures (i.e. filter) to extract pixel-wised features, which causes rain streaks remain in the low-frequency part. JORDER [6] and DID-MDN [24] both generate over-smoothed results due to the redundant signal removal operation. In contrast, the AI-GAN effectively removes rain streaks while preserving texture details based on our decomposition idea and well-designed structure with adversarial training mechanism.

Ablation Studies and User Study: In order to further analyze the efficacy of the proposed signal decomposition idea, asynchronous and interactive network structure, and mutual adversarial optimization mechanism, we also implement three ablated baselines for comparison: (1) *S-GAN*, a single GAN without double branch structure. (2) *D-GAN*, remove the asynchronous synthesis strategy and interaction operation of AI-GAN. (3) *AI-CNN*, remove the GAN loss of AI-GAN during training and propose AI-CNN.

Table 1 shows that AI-GAN achieves 2.49/2.27dB, 2.61 /2.61dB and 1.47/1.49dB higher of PSNR over three ablated

[1] https://sites.google.com/view/reside-dehaze-datasets

Fig. 5. Results of different methods on real-world hazy images: (a) hazy image, (b) DehazeNet [7], (c) MSCNN [8], (d) AOD-Net [9], (e) AI-GAN.

Table 2. PSNR (top) and SSIM (bottom) results of dehazing.

DCP	DehazeNet	MSCNN	AOD-Net	**AI-GAN**
18.95	20.92	21.25	21.66	**22.83**
0.8584	0.8609	0.8744	0.8907	**0.9092**

baselines (S-GAN, D-GAN, and AI-CNN) on Rain100L and Rain100H respectively.

For a more comprehensive qualitative evaluation, we also conduct a user study to demonstrate our models effectiveness in generating visually attractive results. 50 non-expert subjects (assessors) are instructed to vote for the best de-rained results by different methods (Detail-Net[5], JORDER [6], S-GAN, and AI-GAN) based on the perceptual quality considering both rainy artifacts and smoothness. Finally, Detail-Net, JORDER, S-GAN, and AI-GAN gets 5, 111, 68, 316 votes respectively from total 500 votes, which demonstrates AI-GAN's effectiveness in synthesizing more realistic and high-quality de-rained images.

Table 3. PSNR and SSIM results of denoising.

	PSNR				
	BM3D	EPLL	WNNM	DnCNN	**AI-GAN**
σ=15	31.07	31.21	31.37	31.73	**32.33**
σ=25	28.57	28.68	28.83	29.12	**29.75**
σ=50	25.62	25.67	25.87	26.23	**26.88**
	SSIM				
σ=15	0.8721	0.8845	0.8846	0.8954	**0.9113**
σ=25	0.8017	0.8033	0.8160	0.8256	**0.8432**
σ=50	0.6869	0.6994	0.7033	0.7235	**0.7468**

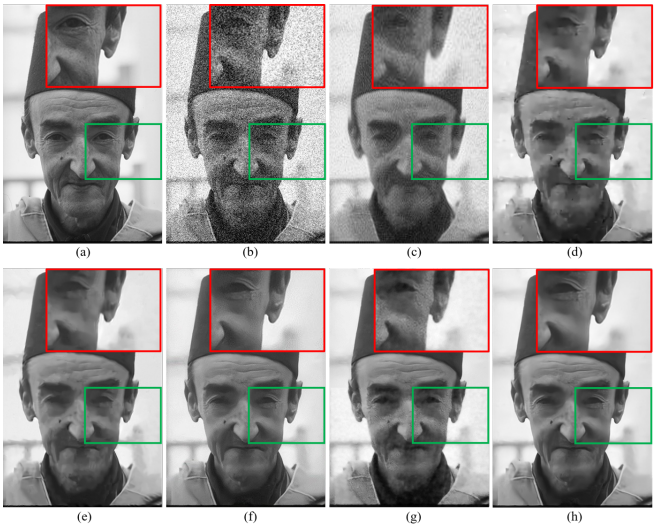

Fig. 6. Results of different methods on the BSD68 dataset with noise level 40. From left to right: (a) Ground Truth (b) noisy image, (c) BM3D [16], (d) EPLL [18], (e) WMMN [19], (f) DnCNN and (g) DnCNN-B [12], (h) AI-GAN.

4.2. Image Dehazing and Denoising

Table 2 and Table 3 display the average PSNR and SSIM values of dehazed and denoised results on the testing set. The experimental results demonstrate that the proposed AI-GAN outperforms other state-of-the-art algorithms. More appealing is the observation that AI-GAN obtains even greater SSIM advantages over all competitors, which verify the demonstration that AI-GAN promises more realistic and high-quality results with more texture details. Subjective comparison results are shown in the Figure 5 and Figure 6, which demonstrate that the proposed AI-GAN has the best power to remove interfering haze or Gaussian noises to the most extent while still preserving texture details in the background scene.

5. CONCLUSIONS AND FUTURE WORK

In this paper, from the novel perspective of signal decomposition, we propose an Asynchronous Interactive Generative Adversarial Network (AI-GAN) to solve the image signal de-interference problems, including image deraining, dehazing, and denoising. AI-GAN decomposes the degraded signal into the original part and the interfering part based on a double branch structure. Each branch further employs an asynchronous synthesis strategy and interacts with each other, achieving a mutual promotion effect. Extensive experiments validate the high efficiency of AI-GAN and the state-of-the-art performance is achieved on the image deraining, dehazing, and denoising task. In the future, we plan to apply AI-GAN to more challenging tasks such as audio denoising and video denoising, and then popularize the signal decomposition idea.

6. ACKNOWLEDGMENTS

This work was supported in part by NSFC under Grant 61571413, 61390514.

7. REFERENCES

[1] Peter C Barnum, Srinivasa Narasimhan, and Takeo Kanade, "Analysis of rain and snow in frequency space," *IJCV*, vol. 86, no. 2-3, pp. 256, 2010.

[2] Li-Wei Kang, Chia-Wen Lin, and Yu-Hsiang Fu, "Automatic single-image-based rain streaks removal via image decomposition," *TIP*, , no. 4, pp. 1742–1755, 2012.

[3] Yu Luo, Yong Xu, and Hui Ji, "Removing rain from a single image via discriminative sparse coding," in *ICCV*, 2015, pp. 3397–3405.

[4] Xin Jin, Zhibo Chen, Jianxin Lin, Jiale Chen, Wei Zhou, and Chaowei Shan, "A decomposed dual-cross generative adversarial network for image rain removal," in *The British Machine Vision Conference (BMVC)*, 2018.

[5] Xueyang Fu, Jiabin Huang, Delu Zeng, Yue Huang, Xinghao Ding, and John Paisley, "Removing rain from single images via a deep detail network," in *CVPR*, 2017.

[6] Wenhan Yang, Robby T Tan, Jiashi Feng, Jiaying Liu, Zongming Guo, and Shuicheng Yan, "Deep joint rain detection and removal from a single image," in *CVPR*, 2017, pp. 1357–1366.

[7] Bolun Cai, Xiangmin Xu, Kui Jia, Chunmei Qing, and Dacheng Tao, "Dehazenet: An end-to-end system for single image haze removal," *TIP*, vol. 25, no. 11, pp. 5187–5198, 2016.

[8] Wenqi Ren, Si Liu, Hua Zhang, Jinshan Pan, Xiaochun Cao, and Ming-Hsuan Yang, "Single image dehazing via multi-scale convolutional neural networks," in *ECCV*. Springer, 2016, pp. 154–169.

[9] Boyi Li, Xiulian Peng, Zhangyang Wang, Jizheng Xu, and Dan Feng, "Aod-net: All-in-one dehazing network," in *ICCV*, 2017, pp. 4770–4778.

[10] Junyuan Xie, Linli Xu, and Enhong Chen, "Image denoising and inpainting with deep neural networks," in *NIPS*, 2012, pp. 341–349.

[11] Viren Jain and Sebastian Seung, "Natural image denoising with convolutional networks," in *NIPS*, 2009.

[12] Kai Zhang, Wangmeng Zuo, Yunjin Chen, Deyu Meng, and Lei Zhang, "Beyond a gaussian denoiser: Residual learning of deep cnn for image denoising," *TIP*, vol. 26, no. 7, pp. 3142–3155, 2017.

[13] Yu Li, Robby T Tan, Xiaojie Guo, Jiangbo Lu, and Michael S Brown, "Rain streak removal using layer priors," in *CVPR*, 2016, pp. 2736–2744.

[14] Kaiming He, Jian Sun, and Xiaoou Tang, "Single image haze removal using dark channel prior," *TPAMI*, vol. 33, no. 12, pp. 2341–2353, 2011.

[15] Gaofeng Meng, Ying Wang, Jiangyong Duan, Shiming Xiang, and Chunhong Pan, "Efficient image dehazing with boundary constraint and contextual regularization," in *ICCV*. IEEE, 2013, pp. 617–624.

[16] Kostadin Dabov, Alessandro Foi, Vladimir Katkovnik, and Karen Egiazarian, "Image denoising by sparse 3-d transform-domain collaborative filtering," *TIP*, vol. 16, no. 8, pp. 2080–2095, 2007.

[17] Priyam Chatterjee and Peyman Milanfar, "Clustering-based denoising with locally learned dictionaries," *TIP*, vol. 18, no. 7, pp. 1438–1451, 2009.

[18] Daniel Zoran and Yair Weiss, "From learning models of natural image patches to whole image restoration," in *ICCV*. IEEE, 2011, pp. 479–486.

[19] Shuhang Gu, Lei Zhang, Wangmeng Zuo, and Xiangchu Feng, "Weighted nuclear norm minimization with application to image denoising," in *CVPR*, 2014.

[20] Jianxin Lin, Yingce Xia, Tao Qin, Zhibo Chen, and Tie-Yan Liu, "Conditional image-to-image translation," in *CVPR*, 2018, pp. 5524–5532.

[21] Xin Jin, Zhibo Chen, Jianxin Lin, Zhikai Chen, and Wei Zhou, "Unsupervised single image deraining with self-supervised constraints," *arXiv preprint arXiv:1811.08575*, 2018.

[22] Jianxin Lin, Tiankuang Zhou, and Zhibo Chen, "Multi-scale face restoration with sequential gating ensemble network," in *AAAI*, 2018.

[23] David Eigen, Dilip Krishnan, and Rob Fergus, "Restoring an image taken through a window covered with dirt or rain," in *ICCV*. IEEE, 2013, pp. 633–640.

[24] He Zhang and Vishal M Patel, "Density-aware single image de-raining using a multi-stream dense network," in *CVPR*, 2018, pp. 695–704.

[25] Ian Goodfellow, Jean Pouget-Abadie, Mehdi Mirza, Bing Xu, David Warde-Farley, Sherjil Ozair, Aaron Courville, and Yoshua Bengio, "Generative adversarial nets," in *NIPS*, 2014, pp. 2672–2680.